Chapter 3

Laser Desorption Ionization Experiments

3.1 Introduction

The first step in demonstrating the Dustbuster's capabilities was simulating dust impacts using laser desorption ionization. The properties of ions produced using laser desorption are somewhat different than those produced in a high-velocity impact, but there are sufficient similarities to make laser desorption a useful method for evaluating instrument performance [1, 2]. For instance, the ionizing ability of light is much greater than that of an impacting particle with the same energy, while the cratering and vaporizing efficiencies are similar. As a result, the ratio of ions to neutrals in the vapor may be different between the two ionization methods. This may result in different space-charge or shielding effects. However, the initial kinetic energies of the ions are roughly the same, approximately 10-30 eV for laser desorption [3-5]. The duration of the laser pulse can be chosen so that it is similar to the duration of an impact ionization event, estimated to be a few nanoseconds [6, 7].

Laser ionization of stainless steel and copper impacts plates, as well as ionization of various mineral samples embedded in copper impact plates, were used for these

studies. The goal of laser desorption ionization experiments was demonstration of the Dustbuster capabilities, in particular mass resolution and sensitivity, and was not intended as a thorough investigation of the laser desorption ionization process. Some of these results have been reported previously [8, 9].

3.2 Experimental Setup

For laser desorption ionization studies the Dustbuster prototype, shown in Figure 3.1, was assembled using the design described in Chapter 2. The reflectron rings and the drift tube were made from type 304 stainless steel. The front grid was a knitted tungsten mesh custom ordered from Kimball Physics (Wilton, NH). Reflectron rings were spot-welded each to three support pieces, which in turn were mounted using alumina rods and spacers. In order to simplify machining and aligning, only a representative section of the impact plate and extraction grid was built, as illustrated in Figure 3.2. The instrument base, an aluminum piece, served as the center point for all mounted components, including the reflectron rings, the impact plate, extraction grid, drift tube, and support rods. The extraction grid was a 70% transmission, 333 wire-per-inch nickel electroformed grid from Buckbee-Mears St. Paul (St. Paul, MN). Attempts to spring-load the extraction grid for tautness were not successful, so the grid was mounted using conducting carbon tabs. The grids at the center of the impact plate and at the beginning of the drift tube were knitted tungsten mesh.

Using adjustable support rods the Dustbuster was mounted onto an 8” vacuum flange. Also mounted onto the flange were a 25-mm MCP detector (comprised of two

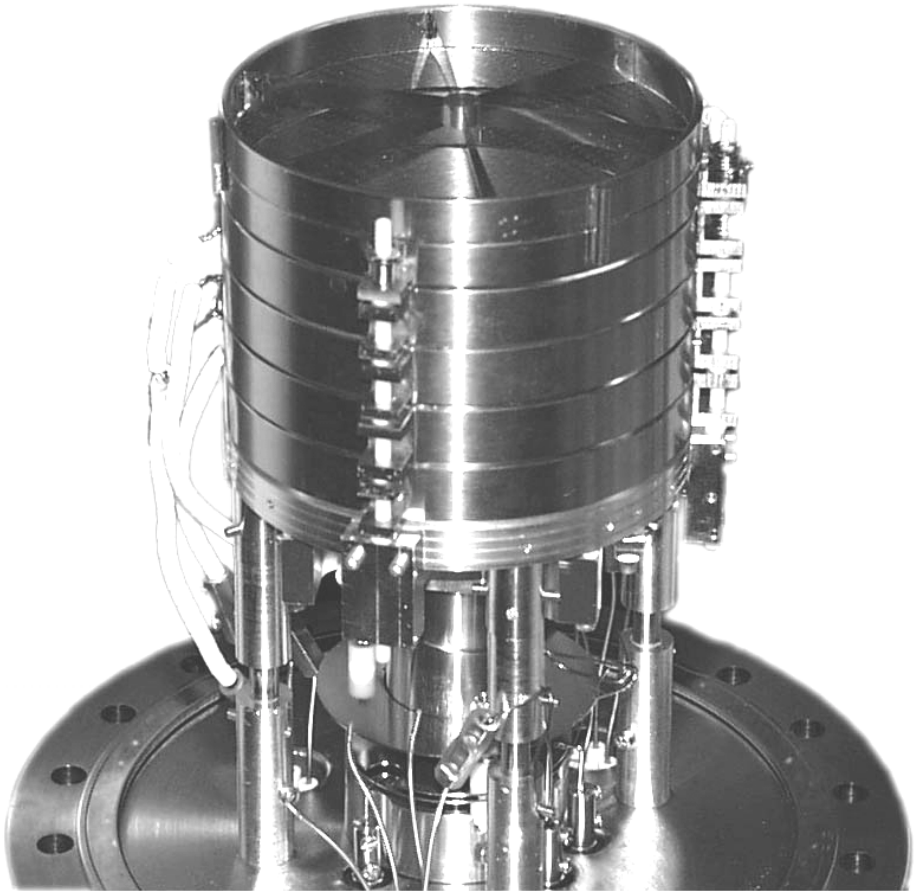

Figure 3.1. Photograph of the Dustbuster prototype used in laser experiments.

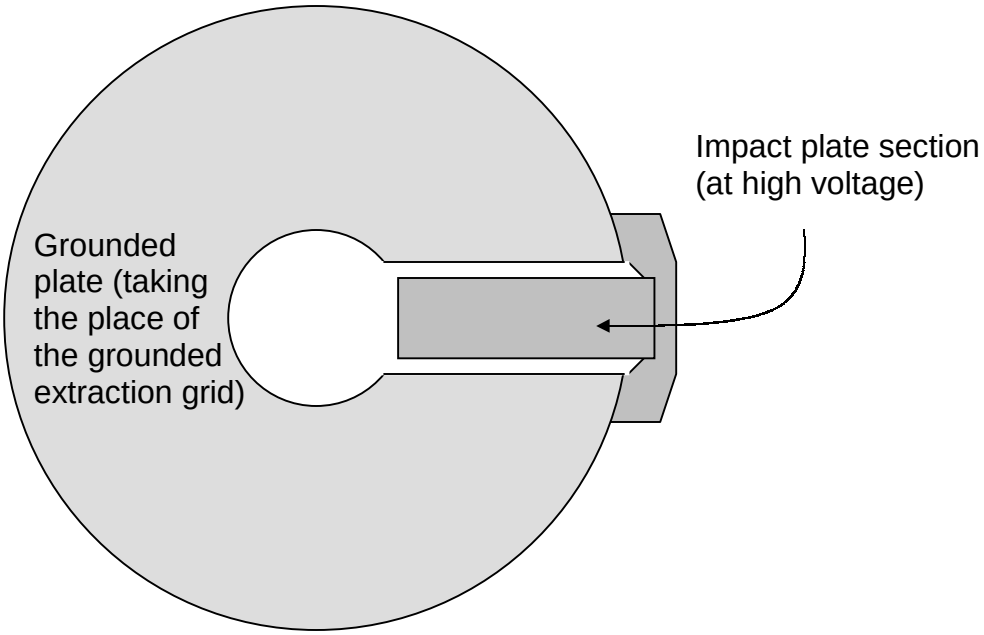

Figure 3.2. Diagram of target plate section used in laser desorption studies of the Dustbuster. Instead of mounting a large grid over the target plate, only a representative section of target plate is used, and is covered with a smaller piece of grid. The extraction grid is mounted on, and connected directly to a grounded plate, which takes the place of the rest of the extraction grid.

stacked plates) and all the electrical feedthroughs needed to provide voltages to the MCP and the Dustbuster electrodes. The mounted MCP detector, purchased from R. M. Jordan, Inc. (Grass Valley, CA) was equipped with a conical anode and impedance-matched (50Ω) connections. The output of the MCP was amplified using an EG&G Ortec fast differentiating pre-amp (model VT120C), which in turn was connected to either a 200 MHz digital oscilloscope (Tektronix) or a 150 MHz digital oscilloscope (Yokogawa).

Voltages for both the MCP plates and the Dustbuster electrodes were produced using two voltage dividers, which in turn were powered by 5 kV power supplies from Stanford Research Systems (Sunnyvale, CA). Although the MCP voltage divider was made from Caddock High Voltage Resistors (Riverside, CA), the other voltage divider was composed of common, inexpensive resistors, arranged so that the voltage across each resistor never exceeded the ratings. The voltage divider made from less expensive resistors seemed to have sufficient stability for the experiment, and no electrical discharges or other problems were observed, even at high voltages.

Figure 3.3 shows the setup for the laser desorption ionization experiments. A 337-nm nitrogen laser (Laser Science, Inc., Franklin, MA) with a pulsewidth of 4 ns was attenuated from 300 μJ to approximately 60 μJ using a variable neutral density filter, although precise laser intensity measurements were not made. Using a bi-convex lens with a focal length of 40 cm, the laser beam was focused to the smallest possible spot size, estimated to be 40 μm, resulting in a power density of 10^8-10^9 W/cm^2. The neutral density filter was varied in order to achieve the best spectra: with too little laser power, spectra showed only alkali metal ions, while too much laser power produced very noisy

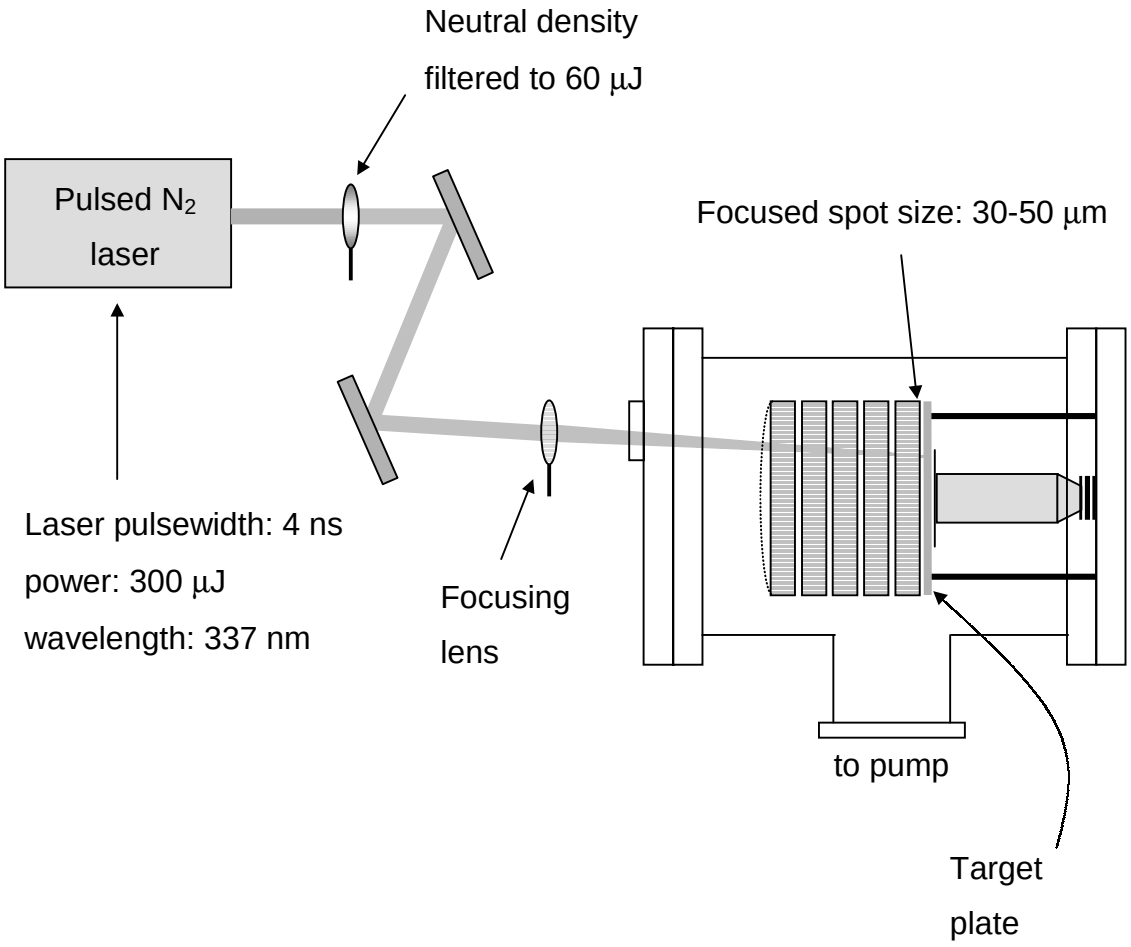

Figure 3.3. Experimental setup for laser desorption ionization experiments on the Dustbuster. Mineral samples were embedded in target plate for some experiments; for others the target plate was made of copper or stainless steel, which acted as the sample.

spectra. At the laser power used in these experiments nearly all species observed were singly charged atomic ions. The Dustbuster was inside a vacuum chamber, which was evacuated by turbopump to below 10^{-7} torr. The position of the focused laser spot was varied over the impact plate in order to simulate impacts at different radii from the instrument axis. However, a careful measurement of spot position was not made. In addition, for mineral samples the laser spot location was limited to the size of the mounted sample, about 5 mm.

For the first laser experiments representative target plate sections were made from type 304 stainless steel and copper. The purity of the copper was not known, although it was probably oxygen-free high-conductivity copper. The steel and copper surfaces were sanded until shiny with 600-grit silicon carbide sandpaper, then degreased and sonicated in HPLC grade methanol. A sputtering source was not available for further surface improvement. In later experiments, mineral samples were mounted onto the copper target plate. Minerals were obtained from the collection of George R. Rossman, Professor of Minerology, Division of Geological and Planetary Sciences, California Institute of Technology, Pasadena, CA. Minerals studied included chalcopyrite ($FeCuS_2$), dolomite ($CaMg(CO_3)_2$), olivine ($(Mg,Fe)_2SiO_4$), and chlorite ($(Mg,Fe)_5(Al,Fe)_2Si_3O_{10}(OH)_8$). For all minerals but dolomite, freshly-cleaved samples, roughly 0.1-0.3 mm thick and 5 mm in diameter, were mounted into recessed holes in the copper plate using adhesive conducting carbon tabs (routinely used for STM work). Of these minerals, only chalcopyrite is electrically conducting. In the cases of the other minerals, the electrical potential at the ionizing surface was not well defined. The depth of the recess in the copper plate corresponded to the thickness of the samples, so that the

mineral surfaces were nearly coplanar with the surface of the copper plate. The dolomite sample did not cleave into a thin piece, but was easily crushed into a powder, which was then pressed onto the adhesive carbon tab.

3.3 Results and Discussion

All laser desorption ionization experiments involved extraction and analysis of positive ions only. Spectra from laser desorption of the stainless steel impact plate were printed out using the Yokagawa oscilloscope printer, but were not recorded in a digital format. Figure 3.4 shows two representative spectra from the steel plate. Note that these are time-domain spectra, so mass scales quadratically, and that the domain is inverted. Ions of sodium and potassium, common contaminants both in laser- and impact-generated ions [6, 10], were observed in all spectra. A peak at m/z = 52, corresponding to $^{52}Cr^{+}$, the principal isotope of chromium (84% of total Cr), was present in all spectra. Type 304 stainless steel is typically 18-20% chromium. The other three stable isotopes of chromium were not clearly observed. Aluminum ion peaks appeared in most of the spectra, but their source is unknown. Neither iron nor the other components of stainless steel were observed, although two spectra showed an unusual group of ion peaks including masses 12, 13, 14, and 15. A few spectra showed small peaks corresponding to hydrogen ions. Appendix A lists all stable, naturally occurring isotopes of all elements observed in the spectra of Chapters 3-5, and includes the masses and natural isotope abundances for each isotope. Accurate estimations of mass resolution were not possible with the steel spectra because of their recorded format.

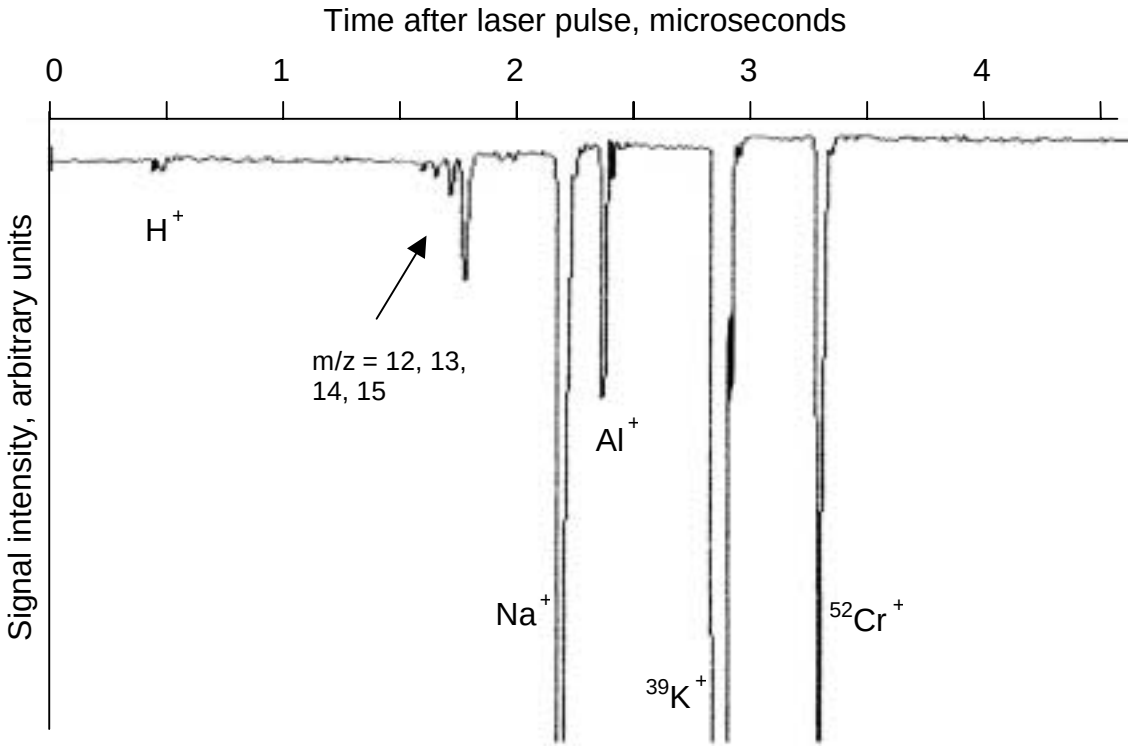

Figure 3.4. Typical laser desorption ionization spectra using a stainless steel target plate. Note that the abscissa is in units of time; mass is not linear on this scale.

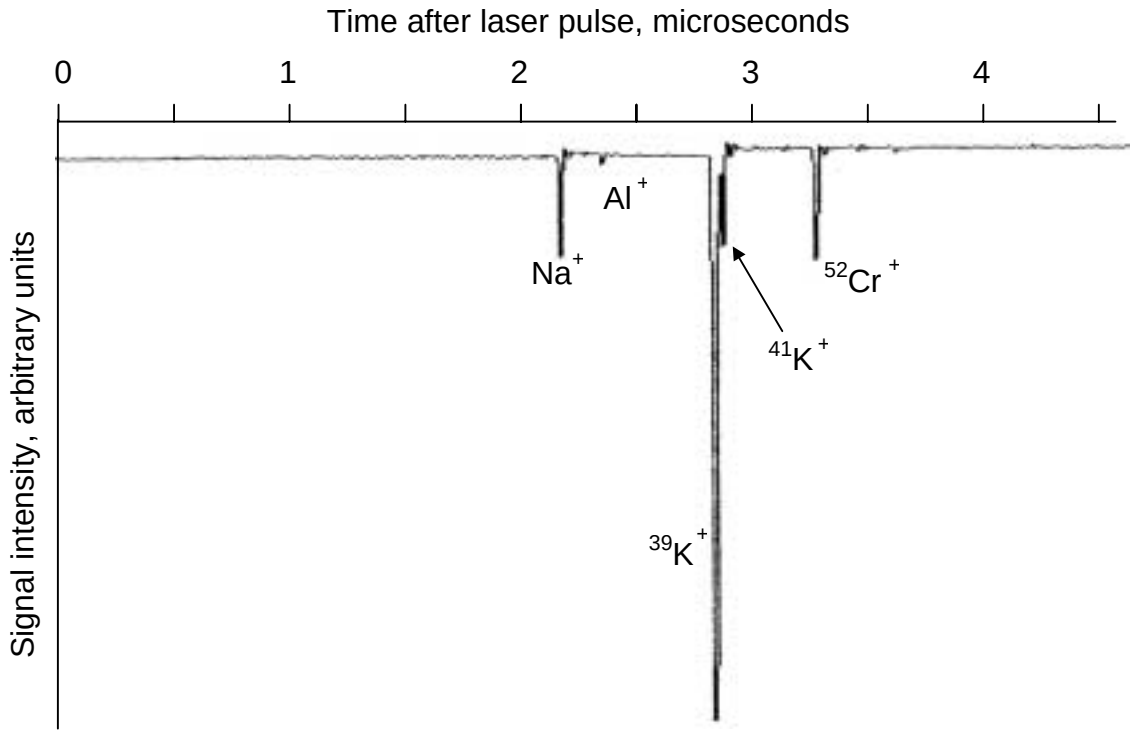

Figure 3.4, continued. Typical laser desorption ionization spectra using a stainless steel target plate. Note that the abscissa is in units of time; mass is not linear on this scale.

Figure 3.5 shows a laser-desorption time-of-flight mass spectrum of the copper target plate. This spectrum is the average of 12 single-shot spectra. Both isotopes of copper are present and completely resolved. Copper cluster ions were also detected. Figure 3.6 shows two representative single-shot spectra using the copper plate. In the averaged spectrum the $^{63}Cu^{+}$ peak has a mass resolution ($m/\Delta m$) of 100. The mass resolution of copper peaks in the individual (single-shot) spectra ranged from 83-150, with an average of 116 and standard deviation of 24. The differences in resolution between shots may be caused by inhomogeneities in the laser beam or the copper surface, or by space-charge effects. The copper isotope ratios, $^{63}Cu/^{65}Cu$, which were measured for each copper spectrum, ranged from 2.3 to 9.3, with an average of 5.4 and standard deviation of 2.45. The value of this ratio should be 2.24 based on natural isotope abundances (see Appendix A). In each case the $^{65}Cu^{+}$ peak is smaller than expected. The small $^{65}Cu^{+}$ peaks appear to be caused by signal overshoot and the slow recovery of the microchannel plate detector.

Figure 3.7 shows an average of 9 spectra from the chalcopyrite ($FeCuS_2$) sample. Figure 3.8 shows two single-shot spectra typical of those observed for chalcopyrite. The chalcopyrite spectra showed a great deal of variability, especially in the relative amounts of copper and iron detected. Other peaks observed include hydrogen, lithium, sodium, aluminum, and potassium. Ions of the principal isotopes of iron, ^{54}Fe and ^{56}Fe, and of copper, ^{63}Cu and ^{65}Cu appeared in most spectra. However, the isotope ratios vary significantly from expected values. The $^{56}Fe/^{54}Fe$ ratio ranged from 9 to 62, although in the latter case the $^{54}Fe^{+}$ peak was small enough to be affected by noise. The average $^{56}Fe/^{54}Fe$ ratio was 16.5, which is close to the expected value of 15.68, based on natural

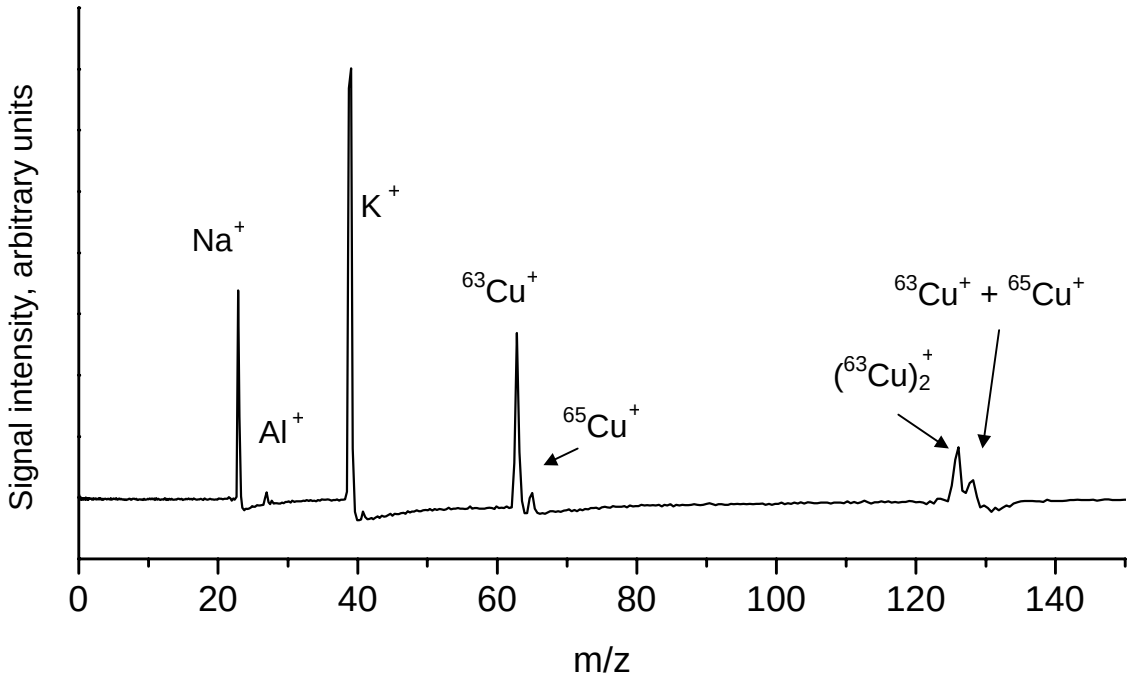

Figure 3.5. Average of 12 laser desorption spectra in which the target plate is copper. Note the presence of both isotopes of copper, as well as the singly charged copper dimer.

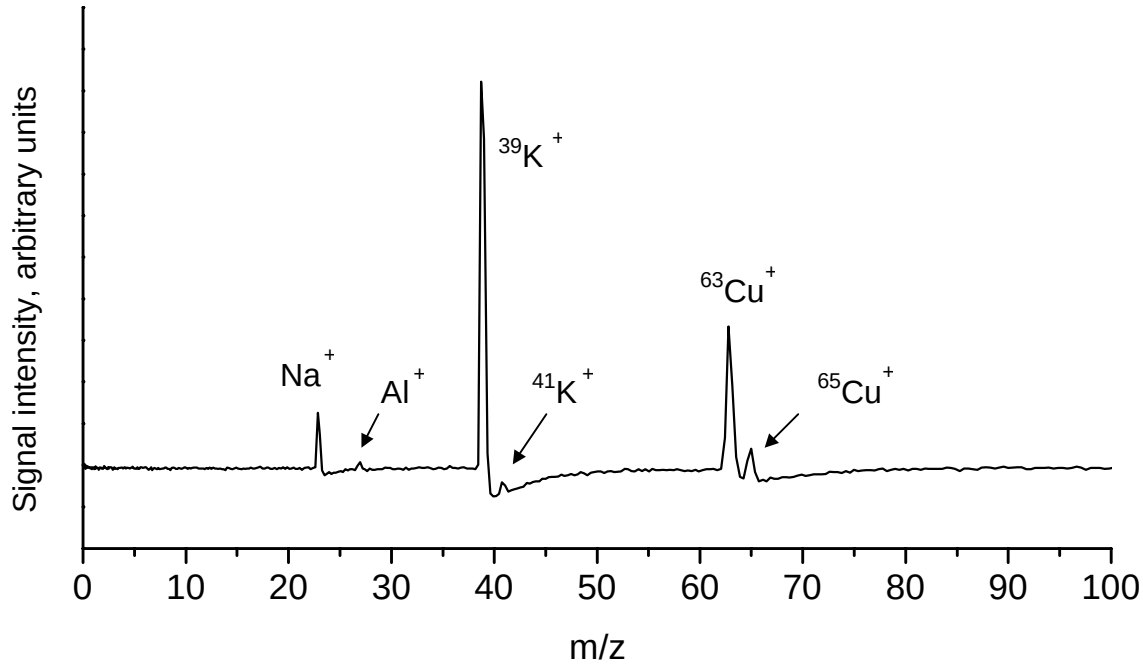

Figure 3.6. Typical single-shot laser desorption ionization spectra of copper target plate.

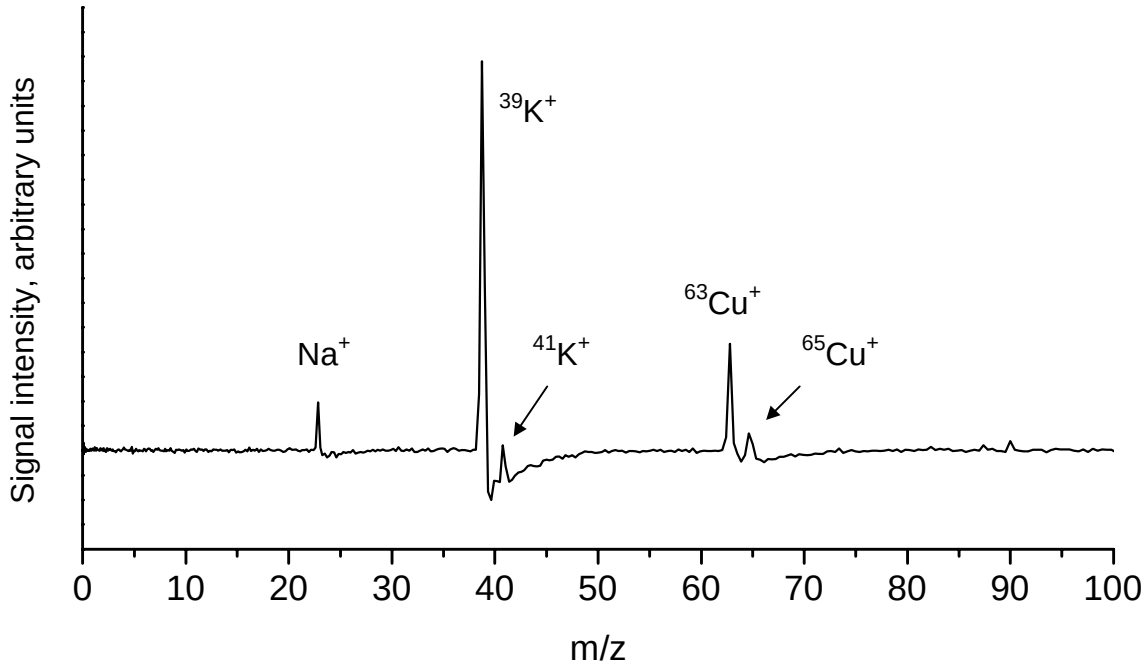

Figure 3.6, continued. Typical single-shot laser desorption ionization spectra of copper target plate.

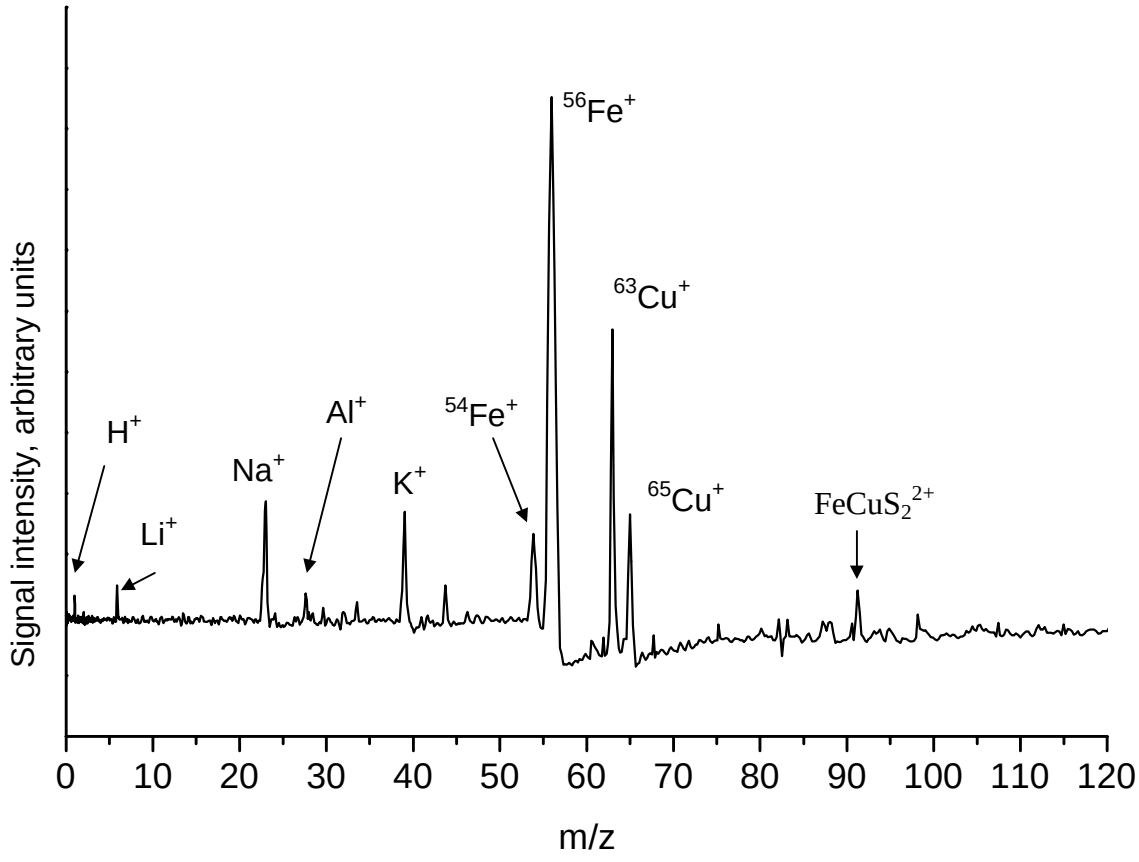

Figure 3.7. Average of nine laser desorption ionization spectra of chalcopyrite, $FeCuS_2$, mounted on target plate.

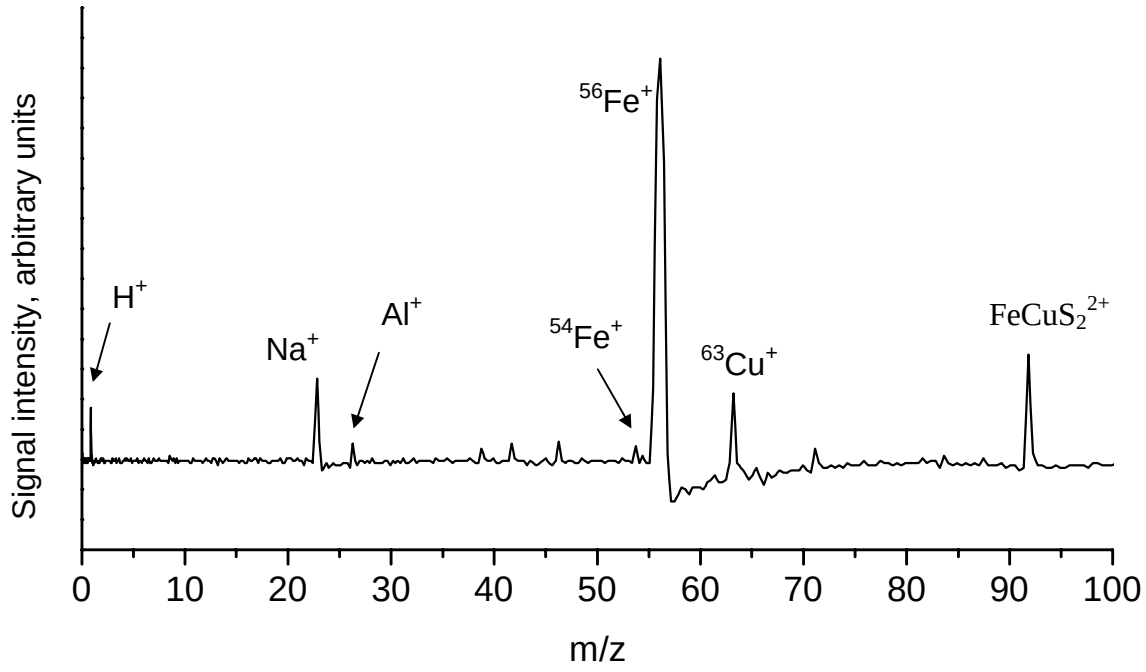

Figure 3.8. Typical single-shot laser desorption ionization spectra of chalcopyrite, $FeCuS_2$.

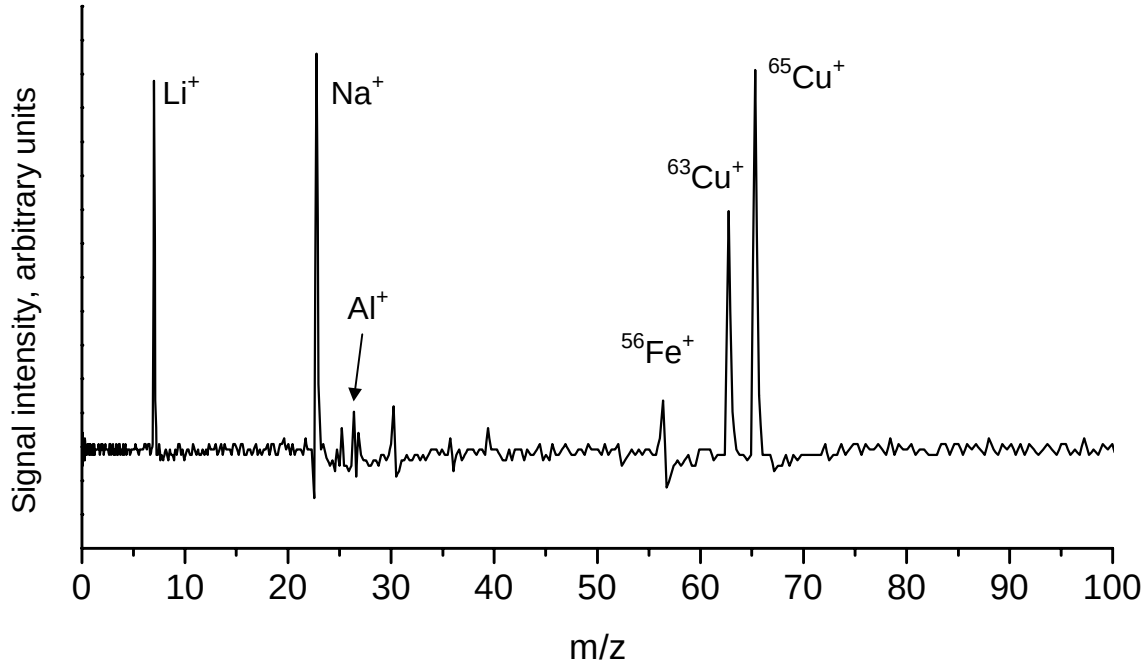

Figure 3.8, continued. Typical single-shot laser desorption ionization spectra of chalcopyrite, $FeCuS_2$.

isotope abundances. The $^{63}Cu/^{65}Cu$ ratio ranged from 0.65 to 3.46. The average $^{63}Cu/^{65}Cu$ ratio was 2.03, close to the expected value of 2.24. In some spectra with weak iron and/or copper signals, the expected intensities of minor isotopes were similar to the intensity of noise peaks, and could not be accurately measured. Chalcopyrite typically does not contain elemental impurities, except occasional zinc [11].

Figure 3.9 shows two typical single-shot spectra from dolomite, $CaMg(CO_3)_2$. The principal isotope of calcium, ^{40}Ca, appears in most spectra. Magnesium is less common. Sodium and potassium appear in most spectra. A peak at 72 appears in most spectra, and could be a species such as CaO_2^+. Some dolomites have impurities of iron, magnesium, or zinc [12].

The chlorites are layered minerals resembling micas. A typical chemical formula for chlorite is $(Mg,Fe)_5(Al,Fe)_2Si_3O_{10}(OH)_8$. The name chlorite is from Greek *chloros*, green, and the mineral does not contain chlorine. Chlorite often contains impurities and trace elements, including Mn, Cr, Ni, Ti, Ca, Na, and K [11]. Figure 3.10 shows two typical single-shot spectra from chlorite. Hydrogen, lithium, and silicon ions appear in some spectra. Various other peaks, some of which are not identifiable, appear sporadically. Most chlorite spectra show several strong, irreproducible peaks at high masses (>100), which are not shown in Figure 3.10. Iron and magnesium ion peaks did not appear at all, and aluminum ions showed up in only one spectrum. The chlorite spectra showed a surprising amount of variation.

Olivine minerals show a great deal of compositional variation, and frequently have impurities of titanium, aluminum, manganese, calcium, sodium, potassium, nickel, chromium, and water [13]. Figure 3.11 shows four typical spectra from olivine,

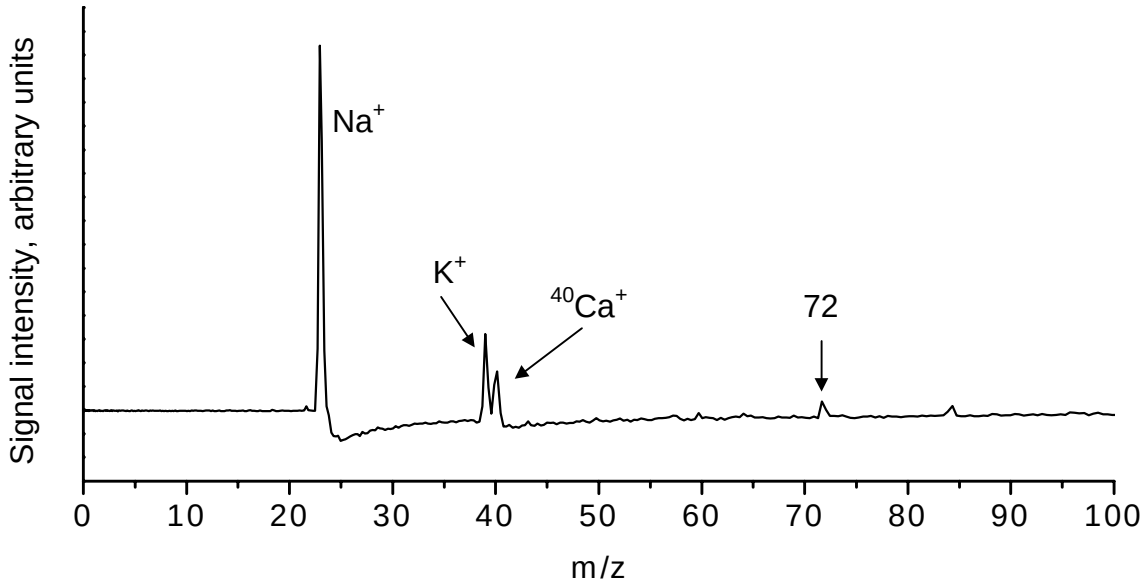

Figure 3.9. Typical single-shot laser desorption ionization spectra of dolomite, $CaMg(CO_3)_2$.

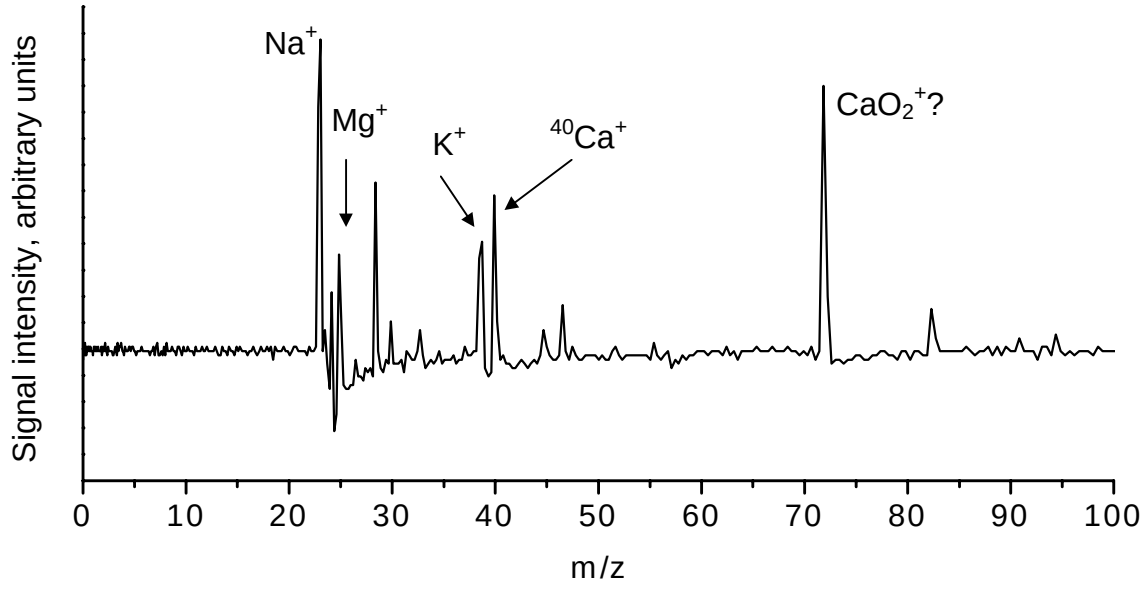

Figure 3.9, continued. Typical single-shot laser desorption ionization spectra of dolomite, $CaMg(CO_3)_2$.

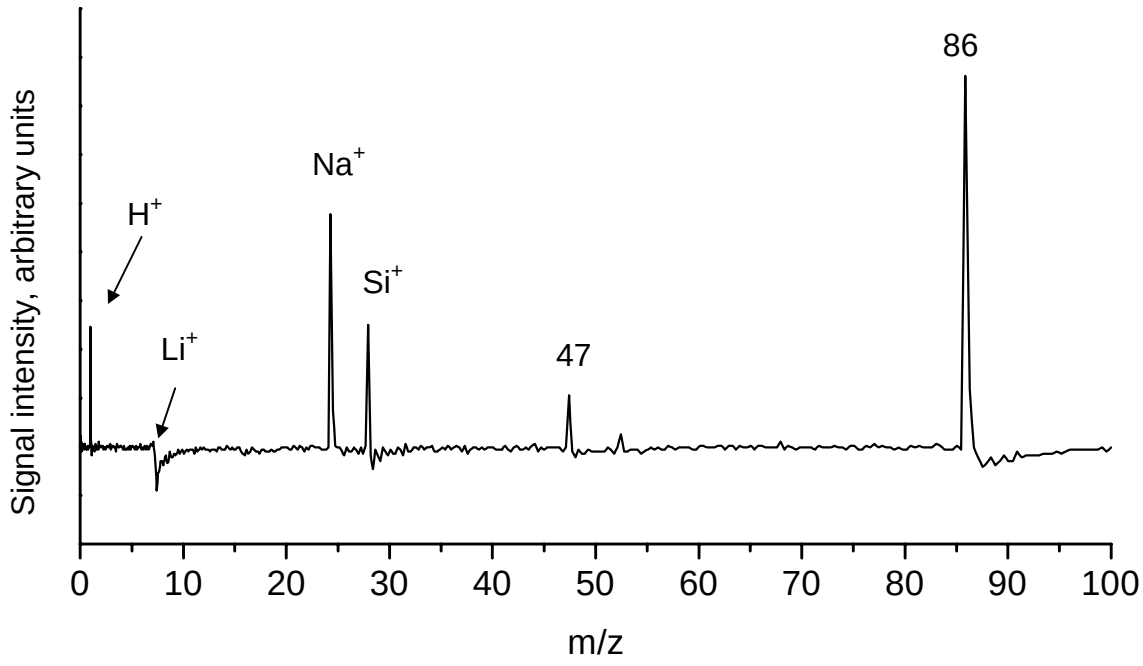

Figure 3.10. Typical single-shot laser desorption ionization spectra of chlorite, $(Mg,Fe)_5(Al,Fe)_2Si_3O_{10}(OH)_8$.

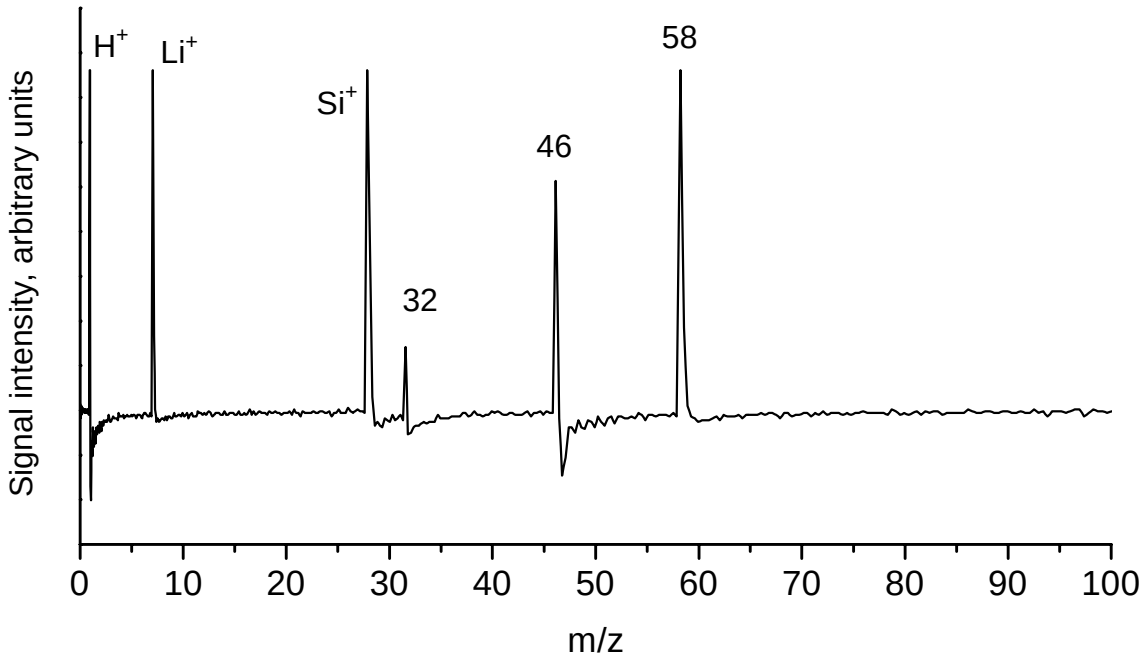

Figure 3.10, continued. Typical single-shot laser desorption ionization spectra of chlorite, $(Mg,Fe)_5(Al,Fe)_2Si_3O_{10}(OH)_8$.

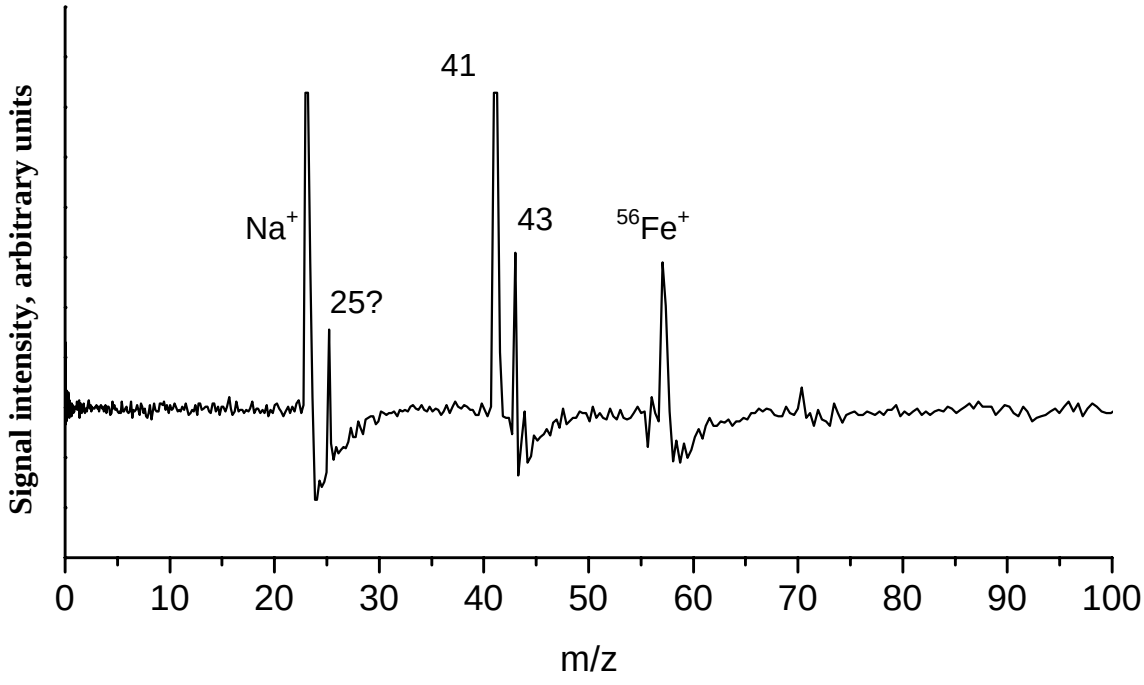

Figure 3.11. Typical single-shot laser desorption ionization spectra of olivine, $(Mg,Fe)_2SiO_4$.

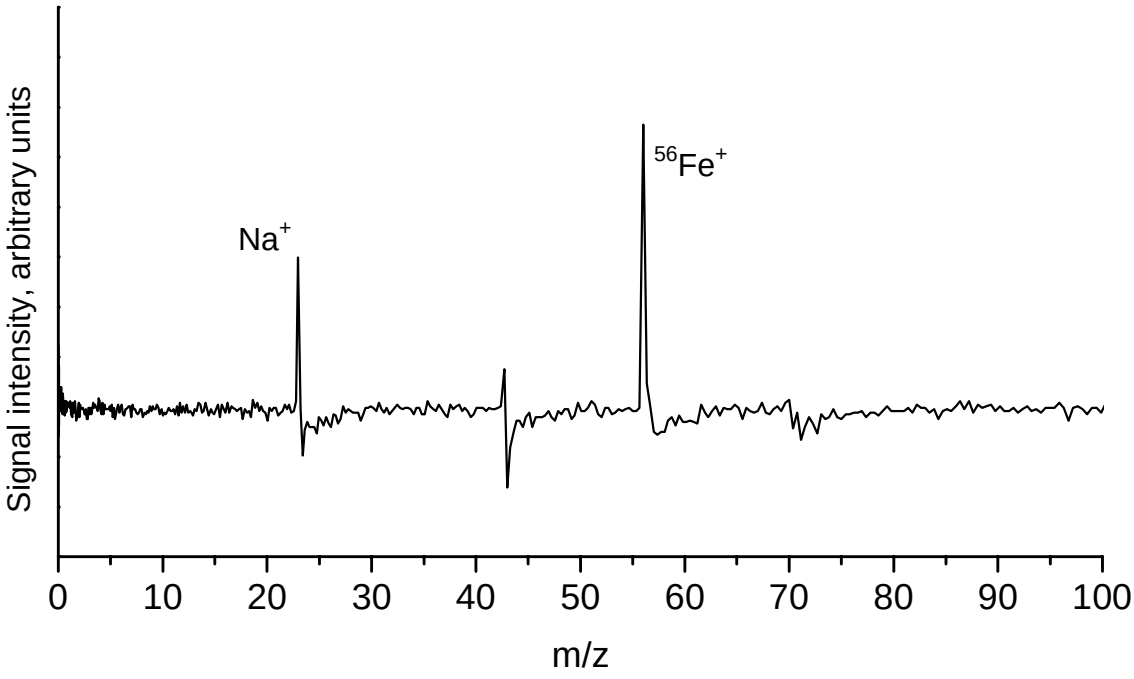

Figure 3.11, continued. Typical single-shot laser desorption ionization spectra of olivine, $(Mg,Fe)_2SiO_4$.

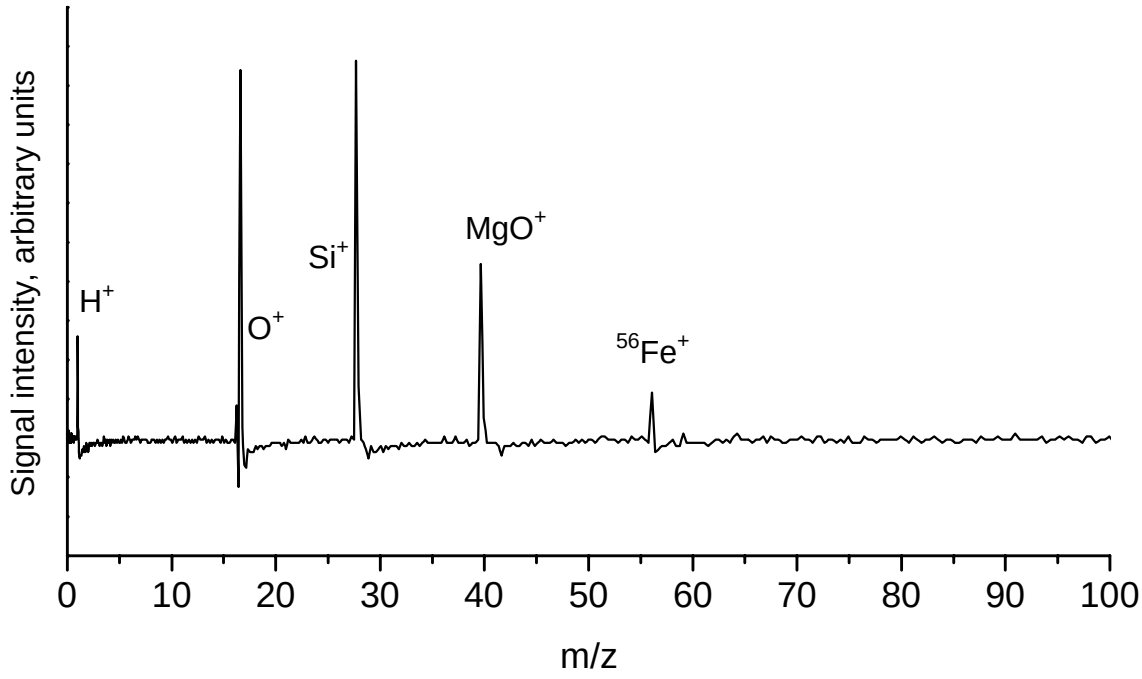

Figure 3.11, continued. Typical single-shot laser desorption ionization spectra of olivine, $(Mg,Fe)_2SiO_4$.

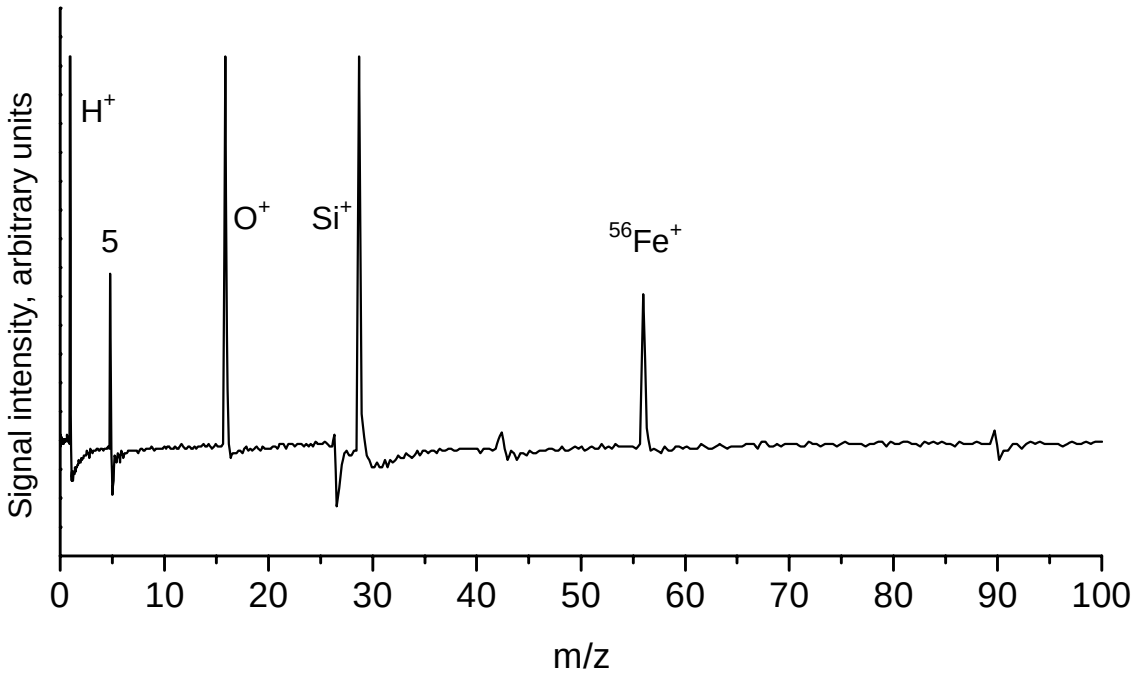

Figure 3.11, continued. Typical single-shot laser desorption ionization spectra of olivine, $(Mg,Fe)_2SiO_4$.

$(Mg,Fe)_2SiO_4$. These spectra also show large variability. Hydrogen, sodium, and silicon ions appear in several spectra each. Oxygen ions are present in some spectra. Although magnesium peaks are absent, iron (^{56}Fe) appears in all spectra. ^{54}Fe is not visible in any spectra. It is possible that the peak at m/z = 56 is something other than iron, such as MgO_2^+ or CaO^+, which might explain the lack of a peak at m/z = 54. Even more unusual is a peak at m/z = 5 which appeared in one spectrum. Because ions originate on an insulating surface with a poorly defined electrical potential, flight times may be skewed, and the normal calibration may not be appropriate. Mass resolution in all the mineral spectra was sufficiently high to resolve isotopes of elements present.

Some of these minerals are semitransparent to visible light, and may be partially transparent to the wavelength of laser used in this experiment. As a result, absorption, ablation, and ionization may be highly inhomogeneous. It is likely that the laser energy is preferentially absorbed by defects and trace metals near the surface of the mineral grains. This may explain the variation and unusual peaks in these spectra, as well as the lack of such peaks as magnesium. Chlorite and olivine, which had the most variation and peculiarities, are also the most transparent. Chalcopyrite is completely opaque to visible light, and dolomite is somewhat opaque.

Isotope ratios varied considerably between shots for each sample examined. In many spectra with iron, $^{54}Fe^+$ was not visible, although it should have been 6% the intensity of the $^{56}Fe^+$ peak. This is clearly not caused by detector saturation because the attenuated peak precedes the large peak in time, but the cause of the anomaly is not known. Averaging several spectra reduces the magnitude of the isotope error for iron, so perhaps the minor isotope peak is simply too small to be seen above the noise in

single-shot spectra. Using an ion detector with a greater dynamic range and sensitivity, such as improved microchannel plates or continuous dynode detectors, will reduce this problem for single-shot spectra. In addition, sources of noise can be identified and reduced.

Laser desorption ionization experiments demonstrate several aspects of the Dustbuster capabilities. Mass resolution is sufficiently high to distinguish isotopes of light elements, at least through copper. Sensitivity is high enough to detect ion signals, although minor isotopes may be difficult to measure. In general, the design seems to work as intended.

3.4 References

1. Kissel, J. and Krueger, F. R., *Ion formation by impact of fast dust particles and comparison with related techniques.* Applied Physics A: Solids and Surfaces, 1987. **42**: p. 69-85.
2. Jyoti, G.; Gupta, S. C.; Ahrens, T. J.; Kossakovski, D.; Beauchamp, J. L., *Mass spectrometer calibration of high velocity impact ionization based cosmic dust analyzer.* International Journal of Impact Engineering, 1999. **23**: p. 401-408.
3. Amoruso, S.; Berardi, V.; Bruzzese, R.; Spinelli, N.; Wang, X., *Kinetic energy distribution of ions in the laser ablation of copper targets.* Applied Surface Science, 1998. **127-129**: p. 953-958.
4. Phipps, C. R. and Dreyfus, R. W., *The High Laser Irradiance Regime: A. Laser Ablation and Plasma Formation*, in *Laser Ionization Mass Analysis*, Vertes, A.; Gijbels, R.; Adams, F., Editors. 1993, Wiley. p. 369-431.

5. Vertes, A.; Juhasz, P.; Jani, P.; Czitrovszky, A., *Kinetic energy distribution of ions generated by laser ionization sources.* International Journal of Mass Spectrometry and Ion Processes, 1988. **83**: p. 45-70.

6. Hansen, D. O., *Mass analysis of ions produced by hypervelocity impact.* Applied Physics Letters, 1968. **13**(3): p. 89-91.

7. Roy, N. L., *Research Investigations of the Physical Interactions and Phenomena Associated with Hypervelocity Sub-micron Particles*. 1975, TRW Systems Group: Redondo Beach, CA. p. 67.

8. Austin, D. E.; Ahrens, T. J.; Beauchamp, J. L., *Dustbuster: a new generation impact-ionization time-of-flight mass spectrometer for in situ analysis of cosmic dust.* Bulletin of the American Astronomical Society, 2000. **32**(3): p. 1043.

9. Austin, D. E.; Ahrens, T. J.; Beauchamp, J. L., *Dustbuster: a compact impact-ionization time-of-flight mass spectrometer for in situ analysis of cosmic dust.* Review of Scientific Instruments, 2002. **73**(1): p. 185-189.

10. Auer, S. and Sitte, K., *Detection technique for micrometeoroids using impact ionization.* Earth and Planetary Science Letters, 1968. **4**: p. 178-183.

11. Deer, W. A.; Howie, R. A.; Zussman, J., *Rock-forming Minerals.* Vol. 3: Sheet Silicates. 1962, New York: Wiley.

12. Chang, L. L. Y.; Howie, R. A.; Zussman, J., *Rock-forming Minerals*. Vol. 5B: Non-silicates: Sulphides, Carbonates, Phosphates, Halides. 1996, Essex: Longman Group.

13. Chang, L. L. Y.; Howie, R. A.; Zussman, J., *Rock-forming Minerals*. Vol. 1A: Orthosilicates. 1982, London: Longman.